## Pyroelectric gating of graphene transistor for plasmon-enhanced optical sensing

Le Wei<sup>1</sup>, Jingjing Qian<sup>1</sup>, Liang Dong<sup>1,\*</sup>, and Meng Lu<sup>1,2,\*</sup>

<sup>1</sup>Department of Electrical and Computer Engineering, Iowa State University, Ames, IA 50011 <sup>2</sup>Department of Mechanical Engineering, Iowa State University, Ames, IA 50011 \*Email: ldong@iastate.edu and menglu@iastate.edu

**Abstract:** A plasmon-enhanced pyroelectric membrane was applied to control the current flow in a graphene transistor for light detection. The graphene transistor was built on a free-standing, 15-μm-thick PVDF membrane, which was doped using gold nanorods to facilitate its optical absorption. Under the resonant condition, the device exhibited a responsivity of 0.79 μA/mW. © 2022 The Author(s)

OCIS codes: (230.0230) Optical device; (140.4780) Optical resonator; (010.1030) Absorption; (250.5403) Plasmonics; (350.5340) Photothermal effects

## 1. Introduction

Pyroelectric materials have been successfully implemented for many applications, such as thermal imaging, gas detection, and chemical composition detection. We report a graphene transistor that uses pyroelectric materials as the gate to regulate current flow between its source and drain terminals. Here, the monolayer graphene was transferred onto a free-standing PVDF-TrFE film, which was doped with gold nanorods (AuNR) as the pyroelectric gate. These AuNRs in the PVDF-TrFE film can help the device absorb visible light within a target spectral range, convert the absorbed optical energy into heat, and effectively raise the membrane temperature. The change of membrane temperature can generate the polarization of the PVDF-TrFE film and tune the graphene film's Fermi level. While the drain-to-source current is a function of excitation flux, the device can be used as an optical sensor.

## 2. Results and discussion

Fig. 1(a) illustrates the pyroelectric material gated graphene field-effect transistor (PG-gFET) device, consisting of a PVDF-TrEF membrane, a monolayer graphene film, metal contacts, and a supporting frame. To effectively convert excitation light into heat, PVDF-TrFE powder was dissolved in dimethylformamide (DMF) and mixed using AuNRs. The localized surface plasmon resonance (LSPR) modes of the AuNRs can boost light absorption and heat the surrounding PVDF-TrFE material quickly. The PG-gFET membrane cross-section optical microscope and scanning electron microscope images are shown in Fig. 1(a). Fig. 1(b) summarizes the major fabrication steps, where the AuNR doped PVDF-TrFE solution was spun onto a graphene-coated copper foil, and the graphene was transferred to the solidified PVDF-TrFE film by etching the copper foil. The PVDF-TrFE membrane with single-layer graphene film was then suspended on a supporting frame. The source and drain contacts were deposited on top of the graphene film.

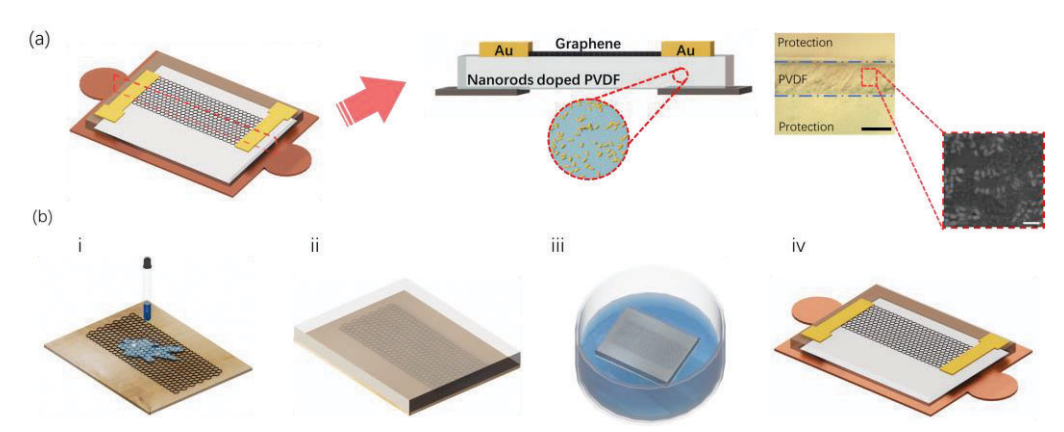


**Fig 1. The PG-gFET device on a PVDF-TrFE membrane.** (a) Schematic diagram of the PG-gFET, right pannel: microscope image of the PG-gFET's cross-section (upper panel, scale bar: 10 μm), and an SEM image of the cross-section with AuNRs (lower panel, scale bar: 200 nm). (b) Major steps for the fabrication of PG-gFET. From i to iv: Spin coating of AuNR doped PVDF-TrFE on graphene, curing PVDF-TrFE, etching of copper, and transferring PG-gFET to a supporting frame.

The PG-gFET was tested using the setup schematically shown in Fig. 2(a), in which the PG-gFET was illuminated by a modulated laser beam to heat and cool the device. The change of  $I_{DS}$  was measured across the source and drain terminals using a current meter. Fig. 2(b) explains how  $I_{DS}$  varies at four consecutive phases of a

heat/cool cycle. During the heating phase, the polarization of the PVDF-TrFE membrane produces a gate potential to shift the Fermi level and increase the current. When the temperature stabilizes, the gate potential disappears, and the current drops back. If the excitation light is turned off, the device starts to cool down, and the temperature change causes another increase of  $I_{\rm DS}$ . When the device temperature completely stabilizes to room temperature,  $I_{\rm DS}$  decreases to the ambient current. Fig. 2(c) plots the device output measured as a function of the time when the laser's intensity was modulated using a 200-ms-period square wave function. The peak current was  $I_{\rm DS,max} = 0.076$  mA with the excitation wavelength, power, and incidence angle of  $\lambda = 650$  nm, P = 90 mW/mm², and  $\theta_{\rm i} = 0^{\circ}$ , respectively, and the PG-gFET voltage was  $V_{\rm DS} = 4$ V. The current output reached its maximum value within 50 ms.

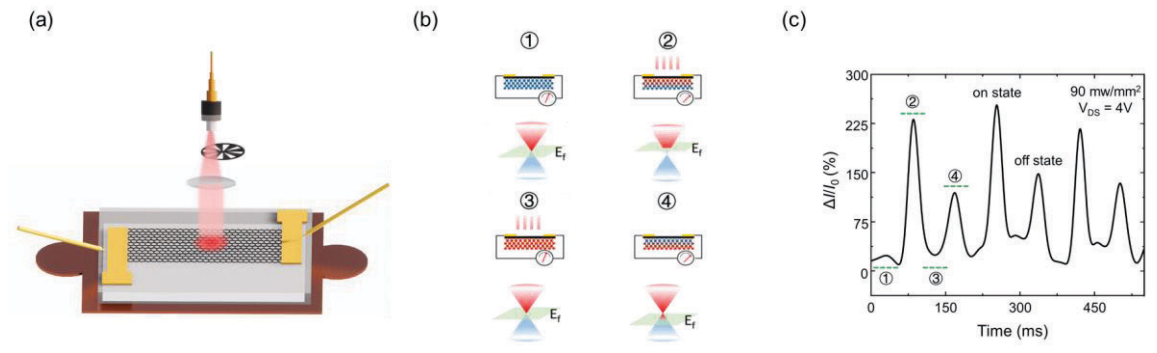


Fig 2. Operation of the PG-gFET detector. (a) Schematics of the PG-gFET detection setup. (b) PG-gFET detection mechanism. (c) Measured current output as a function of time when the intensity-modulated laser beam illuminated the device.

Fig. 3(a) shows the I-V curves of PG-gFET under laser illumination with different excitation power. When the laser power density increased from 0 to 90 mW/mm², the  $I_{DS}$  rose from 0.008 mA to 0.039 mA. The current response ( $I_{DS}$  vs. P) relationship was plotted in the inset of Fig. 3(a). Fig. 3(b) compares the PG-gFETs with two different light-absorbing materials, including a carbon coating on the bottom of the PVDF-TrFE film with AuNRs doped inside. With the same amount of optical absorption (~90 mW/mm²), the AuNR doped device showed a larger current change and an improved signal-to-noise ratio. The carbon coating can heat the membrane from its bottom but is less efficient in photothermal conversion than AuNRs. Owing to the LSPR mode, the optical response of the PG-gFET sensor is wavelength-dependent. Fig. 3(c) shows the spectral response of the device and its LSPR absorption spectrum. At the peak of the LSPR absorption ( $\lambda_r = 660$  nm), the device exhibited a maximum responsitivity of 0.79  $\mu$ A/mW at  $\lambda = 650$  nm. In contrast, the carbon-coated device lacks the capability of distinguishing different wavelengths.

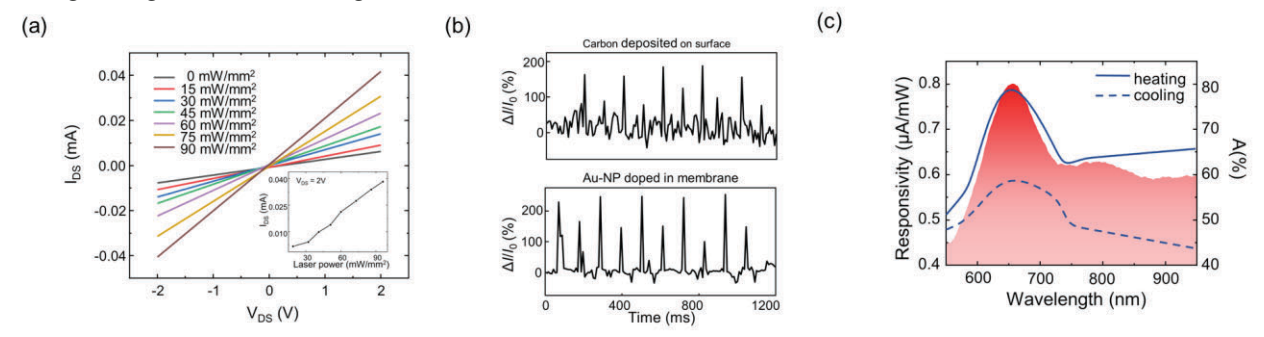


Fig 3. Characterization of the PG-gFET detector. (a) Measured  $I_{DS}$ - $V_{DS}$  curves with different excitation power densities. Inset: the change of  $I_{DS}$  as a function of excitation light power. (b) Current changing response of PG-gFET device using a carbon paint (top) and AuNRs (bottom) as the light absorption material, respectively. (c) Responsivity vs. wavelength during the heating (solid line) and cooling (dashed line) phases, respectively. The red shadow represents the absorbance of the AuNR-doped PVDF-TrFE membrane.

## References:

- Kumar, Mohit, Dong-Kyun Ban, and Joondong Kim. "Photo-Induced Pyroelectric Spikes for Neuromorphic Sensors." Materials Letters 225 (2018): 46-49.
- Pandya, S., G. Velarde, L. Zhang, J. D. Wilbur, A. Smith, B. Hanrahan, C. Dames, and L. W. Martin. "New Approach to Waste-Heat Energy Harvesting: Pyroelectric Energy Conversion." Npg Asia Materials 11 (Jun 7, 2019).
- Wei, L., H. Monshat, J. J. Qian, L. Dong, and M. Lu. "Tunable Resonant-Photopyroelectric Detector Using Chalcogenide-Metal-Fluoropolymer Nanograting." Advanced Optical Materials 9, no. 22 (Nov 2021).
- Yun, Jaeseok, and Min-Hwan Song. "Detecting Direction of Movement Using Pyroelectric Infrared Sensors." IEEE Sensors Journal 14, no. 5 (2014): 1482-89.